PICTURE OF THE MONTH

Vertically Pointing Airborne Doppler Radar Observations of Kelvin–Helmholtz Billows

BART GEERTS AND QUN MIAO

University of Wyoming, Laramie, Wyoming

(Manuscript received 3 September 2009, in final form 14 October 2009)

ABSTRACT

A train of Kelvin–Helmholtz billows in a deep stratiform cloud over a mountain range is documented using data from a high-resolution vertically pointing airborne Doppler radar. The billows had a spacing of 2–2.5 km and a small aspect ratio. The formation and decay of the billows appear to be related to flow acceleration over a mountain.

1. Introduction

Aircraft frequently encounter mild–severe turbulence within stratiform cloud systems associated with extratropical cyclones. The vertical shear of the horizontal wind in these baroclinic systems is typically strong and may be locally large enough to release Kelvin–Helmholtz (KH) instability. The resulting vortices (or KH *billows*) have strong up- and downdrafts and are believed to be a leading source of the turbulence experienced by aircraft in these cloud systems (e.g., Melnikov and Doviak 2008) as well as in clear air above the boundary layer. The local strong updrafts in a stratiform cloud may be several orders of magnitude larger than the system's large-scale ascent rate. Thus, these updrafts may have significant cloud-microphysical effects, causing local pockets of large, rimed particles and/or large supercooled droplets (e.g., Pobanz et al. 1994).

Here we use airborne Doppler radar data to document a series of KH billows that were encountered by chance in a winter storm over Wyoming. Several previous studies have shown imagery of KH billows (or data supporting the presence of such billows), using flight-level data (e.g., Kropfli 1971; Nielsen 1992), profiling Doppler radar data (e.g., Browning and Watkins 1970; Chilson et al. 2003; Luce et al. 2008), vertically pointing frequency-modulated continuous-wave radars (e.g., Atlas et al. 1970; Gossard 1990), profiling cloud lidar data (e.g., Sassen et al. 2007), and cloud photography (e.g., Aberson and Halverson 2006). The radar data presented herein are of exceptionally high resolution, about 30 × 30 m^2 in a vertical cross section, allowing the depiction of KH billows in rare detail.

The radar data are presented in section 2, and a stability analysis based on a radiosonde released in close proximity is described in section 3.

2. Radar data

On 20 February 2009 the University of Wyoming King Air (WKA) flew along a straight line in deep stratiform cloud over complex terrain (Fig. 1). The flight track was aligned precisely with the mean wind direction at flight level (within 2°). Data from the Wyoming Cloud Radar (WCR) aboard the WKA were collected along this track. The WCR is a 95-GHz Doppler radar with several fixed antennas, including a pair of antennas pointing in the nadir and zenith directions. The WCR nadir and zenith reflectivity and Doppler velocity, corrected for aircraft motion, are shown in a vertical cross section along the flight track in Fig. 2. The wind blew from left to right in this section. The underlying terrain is a forested gently sloping mountain range with two peaks near the cross section. These peaks are labeled in Figs. 1 and 2.

The vertical velocity of the echoes tends to be negative (downward) because of the fallout of snow. The gust probe vertical velocity exceeds the average WCR vertical velocity obtained from the nearest gate of the

Corresponding author address: Bart Geerts, Dept. of Atmospheric Sciences, University of Wyoming, Laramie, WY 82071.
E-mail: geerts@uwyo.edu

DOI: 10.1175/2009MWR3212.1

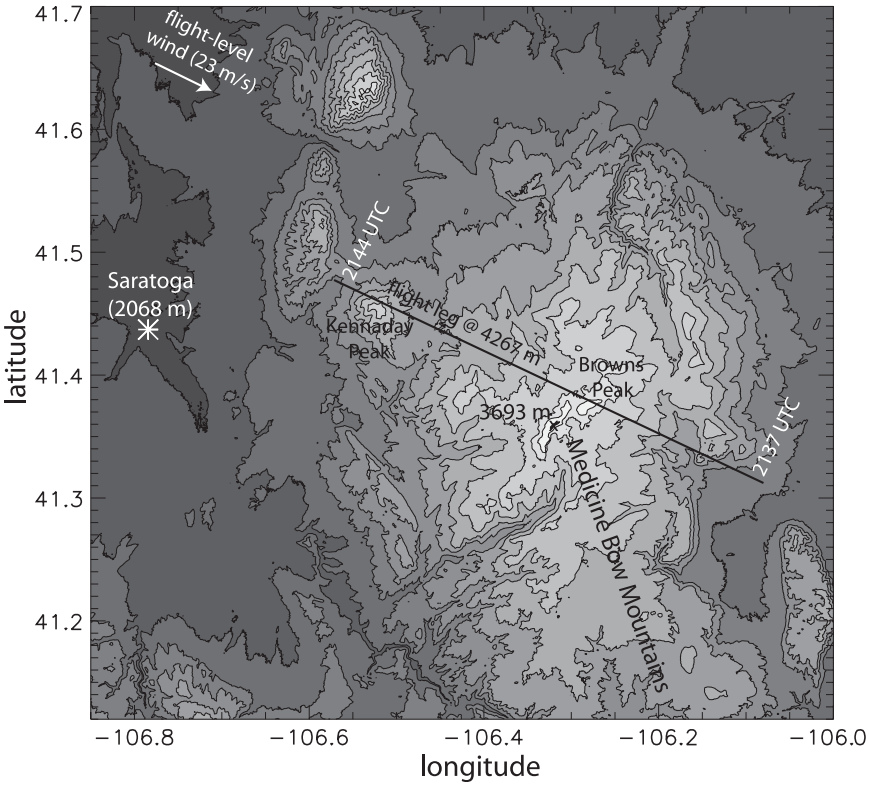

FIG. 1. Topographic map showing location of observations in southeastern Wyoming. Elevations shown are in meters above mean sea level (MSL). The terrain contour interval is 152 m (500 ft).

zenith and nadir antennas (105 m above the aircraft and 120 m below the aircraft) by 1.31 m s^{-1}, on average, for the flight leg shown in Fig. 2. This value can be considered to be the average terminal velocity of the hydrometeors along this track. The actual fall speed probably varied significantly around this average (e.g., Mitchell and Heymsfield 2005). Also, the corrected WCR vertical velocity has a residual uncertainty of ± 0.5 m s^{-1}, due to attitude variations of the aircraft. The variations of the antenna pointing angles from the vertical axis are known but they contaminate the vertical wind field through the horizontal wind profile, which is not known. (Radiosonde and flight-level data are used to remove this contamination from the zenith and nadir Doppler velocities, but some uncertainty remains.) Therefore, we did not subtract the average terminal velocity from the Doppler velocities to obtain the best-guess vertical air motion. We only qualitatively removed the fall speed by centering to color key for vertical velocity at -1.0 m s^{-1}; thus, in essence, blue regions represent updrafts and red regions represent downdrafts.

Much finescale boundary layer turbulence is present near the ground, over a depth of about 1 km. Low-level ascent (descent) is evident upstream (downstream) of terrain ridges, such as Browns Peak. Larger-scale orographic waves are present aloft, around 6 km MSL, with a rising branch near $x = 34$ km and a sinking branch near $x = 50$ km. A downslope windstorm in the lee of Browns Peak is suggested by flow acceleration (Fig. 2c), deep subsidence (Figs. 2b,c), and warming (Fig. 2e).

A train of KH billows can be seen above the flight level, centered near 5.2 km MSL. The billows appear to emerge over Kennaday Peak. The vertical velocity field (Fig. 2b) reveals three–four mostly smooth, coherent eddies that collapse downstream into finescale turbulence (i.e., this appears to be an age-ordered train tied to the terrain). The spacing between the billows is about 2.4 km. The maximum vertical displacement of streamers of higher radar reflectivity and the vertical extent of the up- and downdraft anomalies are roughly 500 m. Thus, the aspect ratio (vertical scale over horizontal scale) of the KH billows is about 1:5. Such small aspect ratio has been observed before for tropospheric KH billows (e.g., Browning 1971), although the value appears to be small relative to numerically simulated KH billows. For instance, the aspect ratio is about 1:2 in Fig. 1 in Fritts et al. (1996). Photographs of KH billows available online suggest a range of aspect ratios between 1:5 and 1:2. Note

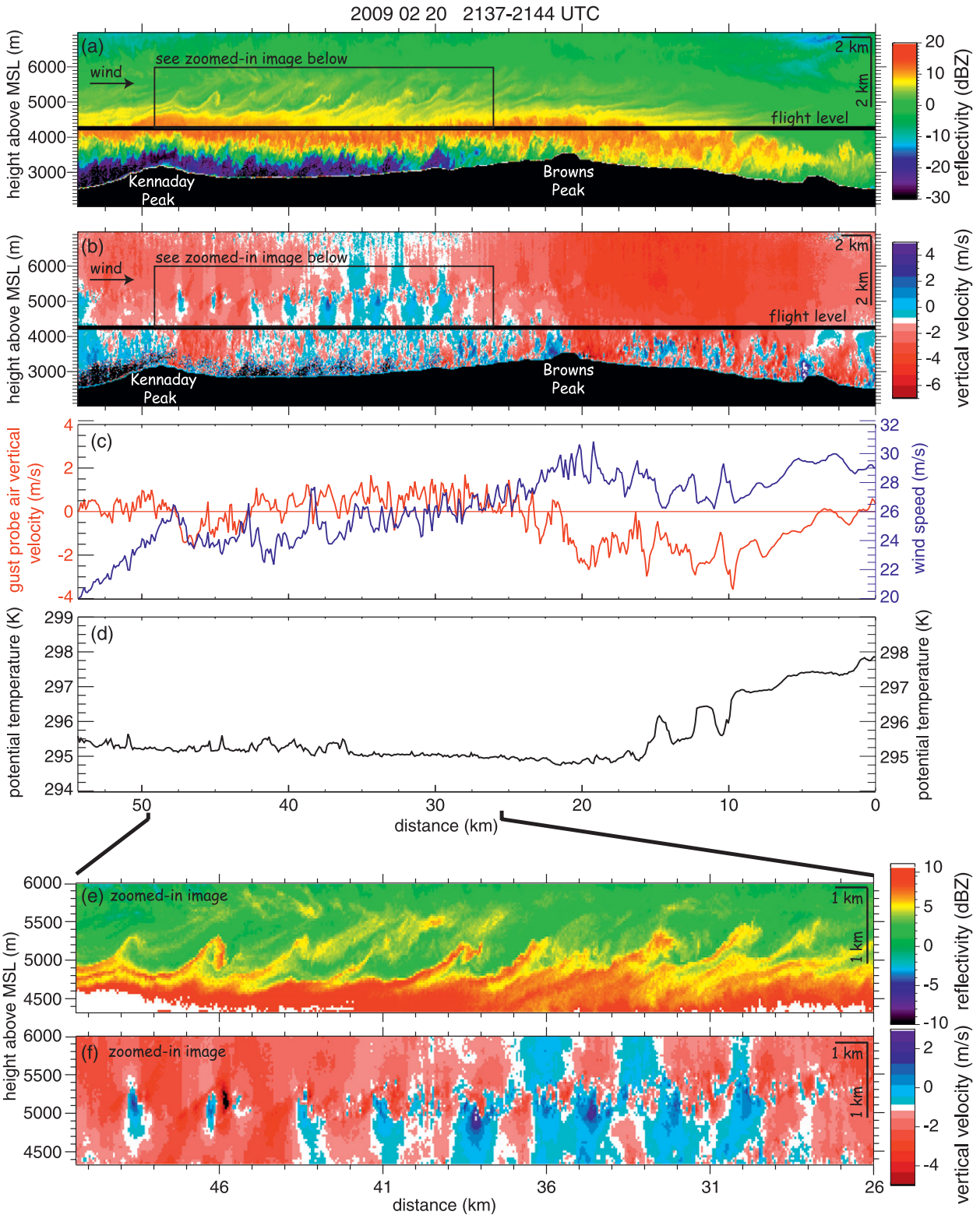

FIG. 2. Profiling radar and flight-level data between 2137 and 2144 UTC 20 Feb 2009. The abscissa is distance from an arbitrary reference point, inferred from GPS data. WCR (a) reflectivity and (b) velocity (positive upward); the thick black horizontal line in (a) and (b) is the radar blind zone surrounding flight level. (c),(d) Flight-level data. (e),(f) A zoomed-in view of the KH billows. Note the change in range of displayed reflectivity and vertical velocity values, intended to highlight the KH billows. Also note that the vertical axis is stretched relative to the horizontal, by a factor of 2.3, in (a)–(d).

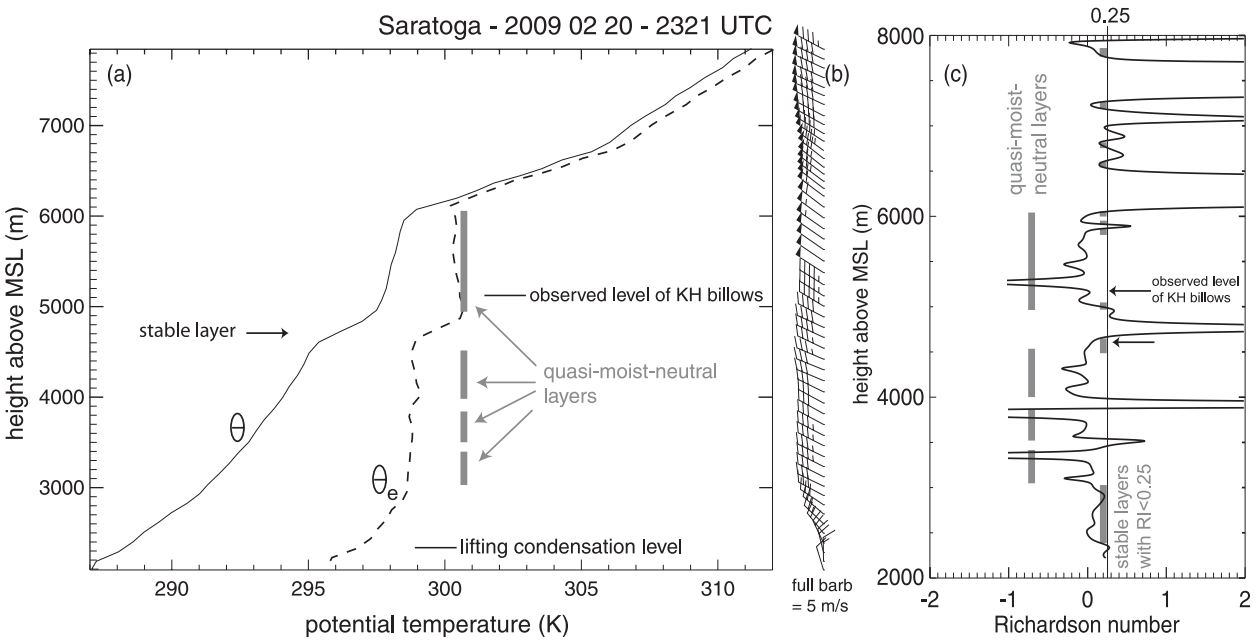

FIG. 3. Profiles based on a radiosonde released from Saratoga at 2321 UTC 20 Feb 2009: (a) potential temperature θ and equivalent potential temperature θ_e; (b) wind; (c) moist Richardson number, smoothed to remove high-frequency (<400 m) variations. Also highlighted in (c) are stable layers in which Ri < 0.25 and quasi-moist-neutral layers.

that the vertical dimension of the radar panels in Fig. 2 is stretched relative to the horizontal dimension.

The higher reflectivity in the streamers may simply be due to advection of larger snow crystals from below. It may also be due to local growth during ascent. Streamers of higher reflectivity can be seen farther downstream than updraft–downdraft pairs associated with a KH billow (Fig. 2a). They become more leveled and stretched out in the downstream direction, especially downstream of Browns Peak. This stretching is probably due to the acceleration of the flow downstream of Browns Peak (Fig. 2c).

The KH billows are shown in more detail in Figs. 2e,f. The vertical velocity pattern is asymmetric because of wave breaking. Even the leading billow lacks the smoothness of a regular wave. The Doppler updrafts (downdrafts) are up to 4 m s^{-1} (−6 m s^{-1}) in strength (i.e., the vertical air motion due to KH instability is as strong as 5 m s^{-1}) although weaker in most billows. The KH updrafts tend to be more local but stronger than the downdrafts. This may explain why the streamers of higher reflectivity are remarkably thin. Behind (to the east of) the fifth KH billow ascent (between x = 35 km and x = 29 km), a number of waves of rising and sinking motion are present in a deep layer, above and below the KH breaking level (Fig. 2f). Their wavelength is about the same as that of the KH billows; therefore, they are probably generated by the billows. The flight level remains below the level of the KH billows and the waves they generated and is at least partially in the turbulent boundary layer. Therefore, the flight-level potential temperature field (Fig. 2d) does not show oscillations coincident with the billows aloft, and the flight-level vertical velocity variations (Fig. 2c) correspond to those in the boundary layer below, measured by the WCR (Fig. 2b).

The winds above Kennaday Peak were strong at flight level, where the wind speed increased from 20 to 26 m s^{-1} from the west end of the transect to Kennaday Peak (Fig. 2c). The horizontal wind below flight level, inferred from dual-Doppler synthesis of the nadir and slant-forward (30° forward of nadir) antenna data (Damiani and Haimov 2006), shows the low-level wind accelerating slightly over Kennaday Peak, and more in the lee of the main crest near Browns Peak, up to ~30 m s^{-1} (not shown). Dual-Doppler synthesis is not possible above flight level, in the region of the KH billows, because there is no slant-forward antenna pointing above the flight level. It is conceivable that the wind speed increased substantially above the level of KH instability, and that this strong wind subsided toward the lee of Browns Peak. Such local increase in wind speed above Kennaday Peak could have spawned the KH billows. This is examined more using radiosonde data in the next section.

3. Stability analysis

A radiosonde was released from Saratoga, Wyoming, (Fig. 1) about 100 min after the flight leg analyzed in Fig. 2. The surface temperature at Saratoga was −5°C.

The low-level backing of the wind, between the surface and 3.0 km MSL (Fig. 3), implies cold-air advection, assuming thermal wind balance. This backing and the high stability in the lowest 1 km are consistent with the passage of a cold front, which was analyzed indeed on the surface weather chart on 0000 UTC 21 February 2009 (not shown).

The cloud base was very low, and there were several quasi-moist-neutral layers above the lowest 1 km and below ~6 km MSL. There was a stable layer between 4.5 and 5.0 km MSL (highlighted with an arrow in Fig. 3a). In this layer the wind speed increased from 17 to 21 m s^{-1}. Following the method of Kirschbaum and Durran (2004), we calculate the Richardson number Ri as follows:

$$\mathrm{Ri} = \frac{\left[\frac{g}{T}\left(\frac{dT}{dz} + \Gamma_m\right)\left(1 + \frac{Lr_s}{R_d T}\right) - \frac{g}{1 + r_s}\frac{dr_s}{dz}\right]}{\left(\frac{d\mathbf{v}}{dz}\right)^2},$$

where r_s is the saturation mixing ratio, Γ_m is the moist-adiabatic lapse rate, L is the latent heat of condensation, R_d is the ideal gas constant for dry air, and $\mathbf{v} = (u, v)$. Both the numerator (the moist Brunt–Vaïsälä frequency squared) and the denominator (the magnitude of the shear squared) of the expression for Ri were first filtered to remove wavelengths shorter than 400 m, before computing their ratio. Some thin layers were slightly potentially unstable ($\partial\theta_e/\partial z < 0$; Fig. 3a). In a number of stable layers Ri < 0.25, the condition for KH instability (e.g., Lin 2008, p. 253). Excluding the quasi-moist-neutral layers, one significant region with Ri < 0.25 is at about 4.6 km MSL (highlighted with an arrow in Fig. 3c). This layer corresponds to the stable layer mentioned above (highlighted with an arrow in Fig. 3a). It is possible that this layer was lifted over the Medicine Bow Range by ~600 m to release KH instability at the observed level of ~5.2 km MSL. As mentioned before, the local winds above Kennaday Peak may have been substantially different than over Saratoga, and the resulting enhanced shear could explain the emergence of KH billows over this mountain.

In summary, the sounding in the upstream valley confirms the presence of a stable layer, although about 600 m below the level of the observed KH billows. The region of packed isentropes may have been lifted over the terrain, and a local maximum in wind shear may have occurred above a peak.

Acknowledgments. We thank the crew of the WKA aircraft—in particular, Jeffrey French—for conducting this flight and for collecting excellent data under rather hazardous conditions. This work was sponsored by the Wyoming Water Research Program.

REFERENCES

Aberson, S. D., and J. B. Halverson, 2006: Kelvin–Helmholtz billows in the eyewall of hurricane Erin. *Mon. Wea. Rev.,* **134,** 1036–1038.

Atlas, D., J. Metcalf, J. Richter, and E. Gossard, 1970: The birth of "CAT" and microscale turbulence. *J. Atmos. Sci.,* **27,** 903–913.

Browning, K. A., 1971: The structure of the atmosphere in the vicinity of large-amplitude Kelvin–Helmholtz billows. *Quart. J. Roy. Meteor. Soc.,* **97,** 283–299.

——, and C. D. Watkins, 1970: Observations of clear air turbulence by high power radar. *Nature,* **227,** 260–263.

Chilson, P. B., T. Y. Yu, R. G. Strauch, A. Muschinski, and R. D. Palmer, 2003: Implementation and validation of range imaging on a UHF radar wind profiler. *J. Atmos. Oceanic Technol.,* **20,** 987–996.

Damiani, R., and S. Haimov, 2006: A high-resolution dual-Doppler technique for fixed multi-antenna airborne radar. *IEEE Trans. Geosci. Remote Sens.,* **42,** 3475–3489.

Fritts, D. C., T. L. Palmer, O. Andreassen, and I. Lie, 1996: Evolution and breakdown of Kelvin–Helmholtz billows in stratified compressible flows. Part I: Comparison of two- and three-dimensional flows. *J. Atmos. Sci.,* **53,** 3173–3191.

Gossard, E. E., 1990: Radar research on the atmospheric boundary layer. *Radar in Meteorology,* D. Atlas, Ed., Amer. Meteor. Soc., 477–527.

Kirschbaum, D. J., and D. R. Durran, 2004: Factors governing cellular convection in orographic precipitation. *J. Atmos. Sci.,* **61,** 682–698.

Kropfli, R., 1971: Simultaneous radar and instrumented aircraft observations in a clear air turbulent layer. *J. Appl. Meteor.,* **10,** 796–802.

Lin, Y.-L., 2008: *Mesoscale Dynamics*. Cambridge University Press, 630 pp.

Luce, H., G. Hassenpflug, M. Yamamoto, S. Fukao, and K. Sato, 2008: High-resolution observations with MU radar of a KH instability triggered by an inertia–gravity wave in the upper part of a jet stream. *J. Atmos. Sci.,* **65,** 1711–1718.

Melnikov, V. M., and R. J. Doviak, 2008: Strong wind shears in stratiform precipitation observed with weather radar. Preprints, *13th Conf. on Aviation, Range, and Aerospace Meteorology,* New Orleans, LA, Amer. Meteor. Soc., 12.4.

Mitchell, D. L., and A. J. Heymsfield, 2005: Refinements in the treatment of ice particle terminal velocities, highlighting aggregates. *J. Atmos. Sci.,* **62,** 1637–1644.

Nielsen, J. W., 1992: In situ observations of Kelvin–Helmholtz waves along a frontal inversion. *J. Atmos. Sci.,* **49,** 369–386.

Pobanz, B. M., J. D. Marwitz, and M. K. Politovich, 1994: Conditions associated with large-drop regions. *J. Appl. Meteor.,* **33,** 1366–1372.

Sassen, K., L. Wang, D. O. Starr, J. M. Comstock, and M. Quante, 2007: A midlatitude cirrus cloud climatology from the Facility for Atmospheric Remote Sensing. Part V: Cloud structural properties. *J. Atmos. Sci.,* **64,** 2483–2501.